k = 14.5 M^{-1} s^{-1} (see Table VI) being of the same order of magnitude as k_{bpy} and k_{phen}.

The sum of experimental findings for the system $[Pd(dtco)_2]^{2+}/mnt^{2-}$ leads to the interpretation that (i) the initial reaction of the anion mnt^{2-} with the cation $[Pd(dtco)_2]^{2+}$ to form the mixed-ligand species [Pd(dtco)(mnt)] is too fast for the stopped-flow time scale (one can estimate $k > 2 \times 10^5$ M^{-1} s^{-1}), (ii) the red neutral intermediate [Pd(dtco)mnt)] with a strong absorption around 520 nm does not precipitate in the stopped-flow experiment because it is formed in low concentration ([Pd(dtco)mnt] = $[Pd(dtco)_2^{2+}]_0$) and, due to the excess condition $[mnt^{2-}]_0 \gg [Pd(dtco)_2^{2+}]_0$, is rapidly converted to the charged green product $[Pd(mnt)_2]^{2-}$ (see Figure 6), and (iii) the reaction of the neutral intermediate with the mnt^{2-} ioon is a second-order reaction following rate law (7) and, most probably, an associative mechanism.

The reaction of the cation $[Pd(dtco)_2]^{2+}$ with the dianion mnt^{2-} is by at least 4 orders of magnitude faster than its reaction with the neutral ligands bpy or phen. Taking into account initial outer-sphere complex formation, one can estimate on the basis of theoretical considerations[27] that the ratio $K_{os}(mnt^{2-})/K_{os}(bpy)$ should be on the order of 100, which would account for part of the rate effect observed. A substantial additional contribution comes probably from the different "nucleophilicity" of the entering ligands, as characterized by their $n_{Pt}°$ values.[27] It is well documented that sulfur-donor ligands such as thiocyanate, dimethyl sulfide or thiourea have much greater $n_{Pt}°$ values than corresponding nitrogen donor ligands, which means that the mnt^{2-} ion, as compared to bpy and phen, is also the "better", i.e., faster reacting nucleophile. In addition, one should keep in mind that the bidentate ligand mnt^{2-} is smaller than bpy and phen and its donor atoms are much more accessible so that coordination in a monodentate fashion is facilitated.

In conclusion, the present contribution provides detailed information on the structural properties of the novel dtco palladium(II) complexes $[Pd(dtco)Cl_2]$ and $[Pd(dtco)_2](NO_3)_2$ and presents data describing the kinetic properties of the species $[Pd(dtco)_2]^{2+}$ in ligand-substitution reactions. As far as the comparison $[M(dtco)_2]^{2+}$ vs $[M(daco)_2]^{2+}$ is concerned one learns that (i) the Cu^{2+} ion oxidizes the thia ligand dtco[20] so that the species $[Cu(dtco)_2]^{2+}$, corresponding to the aza species $[Cu(daco)_2]^{2+}$, is not obtained, (ii) the well-characterized and kinetically studied aza complex $[Ni(daco)_2](ClO_4)_2 \cdot 2H_2O$ has a thia analogue, $[Ni(dtco)_2](ClO_4)_2$,[9] which is thermodynamically not very stable and dissolves with loss of the dtco ligand, (iii) in both complexes $[Pd(dtco)Cl_2]$ and $[Pd(dtco)_2](NO_3)_2$ the cyclic thioether ligand dtco has a folded boat-chair conformation which is practically identical with the conformation of the ring skeleton found for the nickel(II) daco complexes $[Ni(daco)_2]X_2$ (X = ClO_4,[5,6] $B(C_6H_5)_4$[22]), (iv) ligand substitution in the cation $[Pd(dtco)_2]^{2+}$ by bidentate ligands obeys a simple second-order rate law and follows an associative mechanism, and (v) the reaction with even an excess of bpy and phen does not produce the bis complexes but, obviously for steric reasons, only the mixed-ligand species $[Pd(dtco)(bpy)]^{2+}$ and $[Pd(dtco)(phen)]^{2+}$, respectively.

The data presented do not allow a direct comparison of the relative reactivities of two species, $[M(dtco)_2]^{2+}$ and $[M(daco)_2]^{2+}$, in which the same metal cation coordinates either dtco or daco. Work on such a couple of complexes with M = Pd is in progress.

Acknowledgment. Sponorship of this work by the Deutsche Forschungsgemeinschaft and by the Verband der Chemischen Industrie e.V. is gratefully acknowledged. We thank Prof. Dr. E. Wölfel for providing access to the facilities (four-circle diffractometer and computer) of the Stoe & Cie Application Laboratory, Darmstadt, FRG. $PtCl_2$ and $PdCl_2$ were kindly provided by Degussa AG, Frankfurt am Main, FRG.

Supplementary Material Available: Tables SI-SIII, listing complete crystallographic data, calculated coordinates of hydrogens, and thermal parameters, and Table SV, listing the complete set of experimental rate constants (5 pages); Table SIV, listing observed and calculated structure factors (12 pages). Ordering information is given on any current masthead page.

Contribution from the Department of Chemistry, University of California, Davis, California 95616

Ligation-Induced Changes in Metal-Metal Bonding in Luminescent Binuclear Complexes Containing Gold(I) and Iridium(I)

Alan L. Balch* and Vincent J. Catalano

Received May 22, 1990

Treatment of $[Ir(CO)ClAu(\mu\text{-dpm})_2](PF_6)$ (dpm is bis(diphenylphosphino)methane) with 2 or 3 equiv of methyl isocyanide and ammonium hexafluorophosphate yields $[Ir(CNCH_3)_2Au(\mu\text{-dpm})_2](PF_6)_2$ or yellow $[Ir(CNCH_3)_3Au(\mu\text{-dpm})_2](PF_6)_2$, respectively. Red crystals of $[Ir(CNMe)_2Au(\mu\text{-dpm})_2](PF_6)_2 \cdot CH_2Cl_2$ form in the monoclinic space group $P2_1/c$ (No. 14) with a = 20.337 (4) Å, b = 12.633 (2) Å, c = 22.523 (5) Å, and β = 100.29 (1)° at 130 K with Z = 4. Refinement of 4998 reflections and 450 parameters gave R = 0.057 and R_w = 0.055. The structure consists of a nearly planar $Ir(CNCH_3)_2P_2$ unit that is connected to a very linear AuP_2 unit through two dpm bridges. The Ir-Au distance is 2.944 (1) Å. The complex in dichloromethane solution shows a strong absorption at 492 nm (ϵ = 5100 M^{-1} cm^{-1}), which is assigned as the allowed $\sigma^*(d_{z^2}d_{z^2}) \rightarrow \sigma(p_zp_z)$ transition and photoemission at 540 nm (fluorescence) and 668 nm (phosphorescence). Yellow crystals of $[Ir(CNCH_3)_3Au(\mu\text{-dpm})_2](PF_6)_2$ form in the monoclinic space group $C2/c$ with a = 30.511 (8) Å, b = 13.393 (4) Å, c = 28.859 (8) Å, and β = 99.10 (2)° at 130 K with Z = 8. Refinement of 7605 reflections and 462 parameters gave R = 0.0698 and R_w = 0.0534. The structure is similar to that of $[Ir(CNCH_3)_2Au(\mu\text{-dpm})_2](PF_6)_2$ with an isocyanide added to the iridium along the Au-Ir axis. As a result, the Ir-Au distance has *shortened* to 2.817 (1) Å. The contraction is interpreted as resulting from the conversion into a species with an Ir → Au dative bond. The electronic absorption spectrum shows that the proximity-shifted band characteristic of $[Ir(CNMe)_2Au(\mu\text{-dpm})_2](PF_6)_2$ is no longer present. Rather shoulders at 332 (ϵ = 6700 M^{-1} cm^{-1}) and 298 (ϵ = 11000 M^{-1} cm^{-1}) are seen. In dichloromethane at 23 °C, there is a broad emission at 580 nm (with a lifetime of 1.2 μs), which shifts to 628 nm at −196 °C, that is assigned to an excited triplet state.

Introduction

Considerable attention has been given to the spectroscopic and bonding properties of dimeric complexes involving two face-to-face planar d^8 ions. Studies of the absorption spectra and of the long-lived excited states associated with complexes such as $Pt_2(P_2O_5H_2)_4^{4-}$,[1] $Ir_2(\mu\text{-pz})_2(COD)_2$ (pz is pyrazolyl, COD is 1,5-cyclooctadiene),[2] $Rh_2(CNR)_8^{2+}$,[3] and phosphine-bridged Rh(I)

(1) Roundhill, D. M.; Gray, H. B.; Che, C.-M. *Acc. Chem. Res.* **1989**, *22*, 55. Zipp, A. P. *Coord. Chem. Rev.* **1988**, *84*, 47.

0020-1669/91/1330-1302$02.50/0

dimers[4] have produced substantial insight into their electronic structures and reactivities. Additional work on d^{10}–d^{10} dimers has shown that these can also have significant metal–metal interactions that produce luminescent species as well.[5-10] Recently, we reported the first observation of luminescence from a binuclear complex, $[Ir(CO)ClAu(\mu\text{-dpm})_2](PF_6)$ (**1**) (dpm is bis(di-

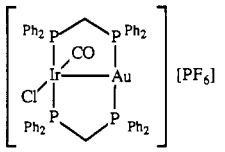

1

phenylphosphino)methane), that incorporates one d^{10} ion (Au(I)) and a d^8 ion (Ir(I)).[11] Complexes of this type are inherently unsymmetrical, and that asymmetry may be expected to produce chemical and spectroscopic properties that are fundamentally different from those of their homobinuclear counterparts. For this reason, we have decided to undertake further studies on these unsymmetrical systems.

In this regard, the work of Shaw and co-workers provides a number of intriguing materials for study. In particular, they report the preparation of a substance, $[Ir(CNBu^t)_3Au(\mu\text{-dpm})_2]Cl_2$, that is clearly related to **1**.[12] However, the structural and spectroscopic studies necessary to determine the nature of the Ir–Au interaction, if any, were not performed. From the proposed structures A and B it appears that the authors did not believe that Ir–Au bonding

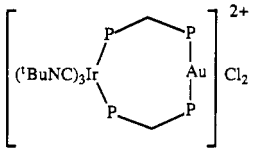

A

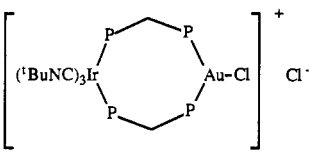

B

was significant in this structure. In this article we describe the structures and electronic spectral features of two closely related complexes whose properties clarify the differing natures of the Au–Ir bonding within each.

Results

Synthetic Studies. As set out in Scheme I, treatment of **1**, prepared by the method of Shaw and co-workers,[13] with 2 equiv of methyl isocyanide in acetone followed by the addition of ammonium hexafluorophosphate in methanol produces crystals of $[Ir(CNCH_3)_2Au(\mu\text{-dpm})_2](PF_6)_2$ (**2**). Solutions of this are green

Scheme I

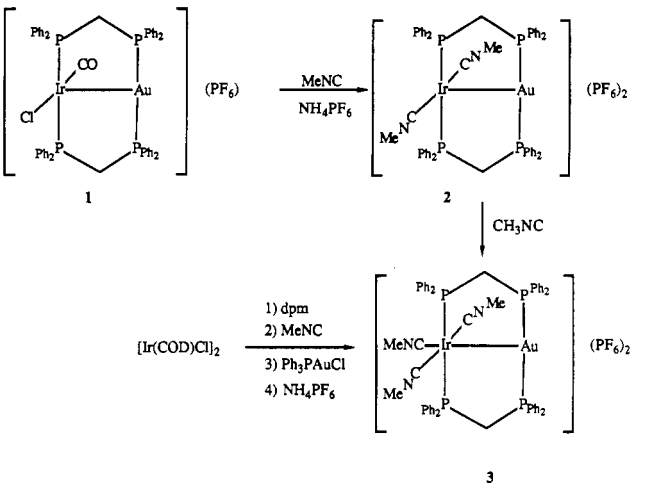

1 **2** **3**

Table I. Selected Interatomic Distances and Angles in $[Ir(CNCH_3)_2Au(\mu\text{-dpm})_2](PF_6)_2$ (**2**) and $[Ir(CNCH_3)_3Au(\mu\text{-dpm})_2](PF_6)_2$ (**3**)

Distances, Å		
	2	**3**
Au–Ir	2.944 (1)	2.817 (1)
Au–P(2)	2.295 (5)	2.292 (5)
Au–P(3)	2.298 (5)	2.280 (5)
Ir–P(1)	2.313 (4)	2.343 (5)
Ir–P(4)	2.339 (4)	2.346 (5)
Ir–C(1)	1.973 (15)	1.99 (2)
Ir–C(3)	1.923 (16)	2.00 (2)
Ir–C(5)		2.09 (2)
P(1)···P(2)	3.099 (9)	3.075 (8)
P(3)···P(4)	3.108 (9)	3.111 (8)
Angles, deg		
	2	**3**
P(2)–Au–P(3)	168.2 (2)	159.2 (2)
P(2)–Au–Ir	96.3 (1)	99.8 (1)
P(3)–Au–Ir	92.4 (1)	101.0 (1)
P(1)–Ir–P(4)	177.7 (1)	158.2 (2)
C(1)–Ir–C(3)	170.3 (6)	169.1 (9)
P(1)–Ir–Au	87.5 (1)	79.1 (1)
P(4)–Ir–Au	91.5 (1)	79.2 (1)
C(1)–Ir–Au	78.6 (4)	84.8 (7)
C(3)–Ir–Au	110.6 (5)	84.7 (6)
P(1)–Ir–C(1)	89.1 (5)	93.1 (6)
P(1)–Ir–C(3)	88.2 (5)	87.7 (6)
P(4)–Ir–C(1)	92.7 (5)	83.5 (6)
P(4)–Ir–C(3)	90.2 (5)	91.7 (6)
C(5)–Ir–Au		177.6 (6)
C(5)–Ir–P(1)		101.1 (6)
C(5)–Ir–P(4)		100.7 (6)
C(5)–Ir–C(1)		97.6 (9)
C(5)–Ir–C(3)		92.9 (8)
Ir–C(1)–N(1)	174.8 (13)	173 (2)
Ir–C(3)–N(2)	172.8 (13)	174 (2)
Ir–C(5)–N(3)		175 (2)

yellow in color. The solid is straw color under natural light, but green under fluorescent lighting. The infrared spectrum shows an absorption at 2179 cm^{-1} (dichloromethane solution) for the two terminal isocyanaide ligands. The $^{31}P\{^1H\}$ NMR spectrum (in $CDCl_3$) shows an AA′XX′ pattern with only 10 of the expected 20 lines observed. Analysis yields δ_A = 32.2 ppm, δ_X = 8.8 ppm and $J(P_AP_X)$ = 33 Hz, $J(P_{A'}P_X)$ = 13 Hz, and a large trans coupling constant in the 100–300-Hz range. Since only a limited number of transitions were observable, it was not possible to evaluate $J(A,A')$ and $J(X,X')$ (i.e. the trans P,P coupling constant) further. The ^1H NMR spectrum in chloroform-*d* shows a singlet at 26.4 ppm for the methyl isocyanide protons and a broad resonance at 4.13 ppm for the methylene protons of the bridging diphosphine.

(2) Marshall, J. L.; Stobart, S. R.; Gray, H. B. *J. Am. Chem. Soc.* **1984**, *106*, 3027. Caspar, J. V.; Gray, H. B. *J. Am. Chem. Soc.* **1984**, *106*, 3029.
(3) Mann, K. R.; Gordon, J. G., II; Gray, H. B. *J. Am. Chem. Soc.* **1975**, *97*, 3553. Mann, K. R.; Lewis, N. S.; Williams, R. M.; Gray, H. B.; Gordon, J. G., II *Inorg. Chem.* **1978**, *17*, 828.
(4) Balch, A. L. *J. Am. Chem. Soc.* **1976**, *98*, 8049. Balch, A. L.; Tulyathan, B. *Inorg. Chem.* **1977**, *16*, 2840. Fordyce, W. A.; Crosby, G. A. *J. Am. Chem. Soc.* **1982**, *104*, 985. Balch, A. L.; Fossett, L. A.; Nagle, J. K.; Olmstead, M. M. *J. Am. Chem. Soc.* **1988**, *110*, 6732.
(5) Casper, J. V.; Gray, H. B. *J. Am. Chem. Soc.* **1988**, *110*, 2145.
(6) Khan, M. N. I.; Fackler, J. P., Jr.; King, C.; Wang, J. C.; Wang, S. *Inorg. Chem.* **1988**, *27*, 1672.
(7) Che, C. M.; Wong, W.-T.; Lai, T.-F.; Kwong, H.-L. *J. Chem. Soc., Chem. Commun.* **1989**, 243.
(8) King, C.; Wang, J.-C.; Khan, M. N. I.; Fackler, J. P., Jr. *Inorg. Chem.* **1989**, *28*, 2145.
(9) Che, C.-M.; Kwong, H.-L.; Yam, V. W.-W.; Cho, K. C. *J. Chem. Soc., Chem. Commun.* **1988**, 885.
(10) Jaw, H.-R, C.; Savas, M. M.; Rogers, R. D.; Mason, W. R. *Inorg. Chem.* **1989**, *28*, 1028.
(11) Balch, A. L.; Catalano, V. J.; Olmstead, M. M. *Inorg. Chem.* **1990**, *29*, 585.
(12) Langrick, C. R.; Shaw, B. L. *J. Chem. Soc., Dalton Trans.* **1985**, 511.
(13) Hutton, A. T.; Pringle, P. G.; Shaw, B. L. *Organometallics* **1983**, *2*, 1889.

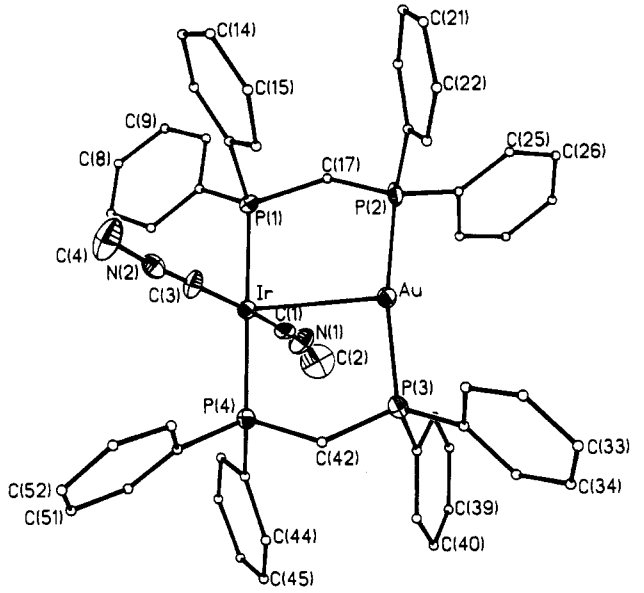

Figure 1. Structure of the cation in $[Ir(CNMe)_2Au(\mu\text{-dpm})_2](PF_6)_2$ (**2**) with 50% thermal contours for the heavy atoms and isocyanide ligand and uniform, arbitrarily sized circles for the carbon atoms of the dpm ligands.

Addition of 1 equiv of methyl isocyanide to **2** in acetone (or 3 equiv to **1**) produces a yellow solution from which yellow crystals of $[Ir(CNMe)_3Au(\mu\text{-dpm})_2](PF_6)_2$ (**3**) may be obtained by precipitation with methanolic ammonium hexafluorophosphate. This complex may also be obtained in a one-step synthesis by the successive additions of appropriate amounts of dpm, methyl isocyanide, Ph_3PAuCl, and ammonium hexafluorophosphate to $[Ir(COD)Cl]_2$. This latter procedure is patterned on the original preparation of $[Ir(CNBu^t)_3Au(\mu\text{-dpm})_2]Cl_2$.[12] The infrared spectrum of **3** in a Nujol mull shows two bands at 2230 (w) and 2201 (s) cm^{-1} for the terminal isocyanide ligands. The $^{31}P\{^1H\}$ NMR spectrum shows an AA'XX' spectrum similar to that reported for the *t*-butyl analogue[12] with 16 of the expected 20 lines observed. Analysis yields δ_A = 47.2 ppm, δ = 7.5 ppm, $J(P_A,P_X)$ = 114 Hz, $J(P_A,P_{X'})$ = −7.0 Hz, $J(P_A,P_{A'})$ = 260 Hz, and $J(P_X,P_{X'})$ = 151 Hz. The ^1H NMR spectrum in chloroform-*d* shows two resonances at 2.51 and 2.97 ppm with integrated intensities of 2:1 for the methyl isocyanide ligands and broad resonance at 4.69 ppm for the methylene protons of dpm.

Structure of $[Ir(CNCH_3)_2Au(\mu\text{-dpm})_2](PF_6)_2\cdot CH_2Cl_2$. The asymmetric unit of $[Ir(CNCH_3)_2Au(dpm)_2](PF_6)_2$ contains the cation, two entirely normal hexafluorophosphate anions, and one molecule of dichloromethane. There are no unusual interactions between these moieties. The structure of the cation as determined by X-ray diffraction studies is shown in Figure 1. Selected interatomic distances and angles are presented in Table I. Atomic coordinates are given in Table II.

The cation consists of a nearly planar $IrP_2(CNMe)_2$ unit that is attached to a nearly linear AuP_2 unit through the two dpm bridges. The eight-membered ring made up of the two metal ions and the two dpm ligands adopts a chair conformation with the four phosphorus atoms nearly coplanar. Consequently, the dihedral angles formed by the P(2)AuIrP(1) and P(3)AuIrP(4) units are small (4.5° and 5.6°, respectively). These are best seen in Figure 2, which shows the core of the cation from a different perspective.

The Ir–Au distance is 2.944 (1) Å. This distance is slightly longer than the range of Ir–Au single bond distances (2.59–2.81 Å).[14-20] It is 0.04 Å shorter than the corresponding distance in $[Ir(CO)ClAu(\mu\text{-dpm})_2]^+$[11] and is shorter than the Au–Ir distances in the nearly linear Ir–Au–Ir and Au–Ir–Au chains in $[Ir_2(CO)_2Cl_2Au(\mu\text{-dpma})_2]^+$ (3.059 (1) and 3.012 (1) Å)[19] and $[Au_2Ir(CO)Cl(\mu\text{-dpma})_2]^{2+}$ (3.013 (2) and 3.014 (2) Å)[20] (dpma is bis((diphenylphosphino)methyl)phenylarsine). The Ir–Au distance is shorter than the nonbonded P···P separations within the two dpm ligands (P(1)···P(2), 3.099 (8) Å and P(3)···P(4), 3.108 (8) Å). Generally, such a difference between the metal–metal separation and the P···P separation in complexes containing a $M_2(\mu\text{-dpm})_2$ core has been taken to indicate an attractive interaction exists between the two metal centers. All other bond distances fall within normal ranges.

The gold ion lies slightly off to one side of the IrP_2C_2 plane toward C(1). Thus the angle between the normal to the IrP_2C_2 plane and the Ir–Au line is 12°. A similar situation exists in $[Ir(CO)ClAu(\mu\text{-dpm})_2]^+$, where the gold ion is displaced slightly

Table II. Atomic Coordinates (×10⁴) and Isotropic Thermal Parameters (Å² × 10³) for $[Ir(CNCH_3)_2Au(\mu\text{-dpm})_2](PF_6)_2\cdot CH_2Cl_2$[a] (**2**)

	x	*y*	*z*	*U*[b]
Au	3084 (1)	5677 (1)	7457 (1)	18 (1)*
Ir	1913 (1)	7068 (1)	7402 (1)	15 (1)*
Cl(1)	3042 (4)	3572 (6)	313 (3)	84 (2)
Cl(2)	4419 (4)	3960 (6)	851 (3)	93 (2)
P(1)	2397 (2)	8171 (3)	6782 (2)	18 (1)*
P(2)	3579 (2)	6621 (4)	6785 (2)	20 (1)*
P(3)	2648 (2)	4436 (4)	8024 (2)	21 (1)*
P(4)	1460 (2)	5967 (3)	8060 (2)	17 (1)*
N(1)	1418 (7)	5647 (11)	6286 (6)	29 (5)*
N(2)	2137 (6)	8859 (11)	8347 (6)	22 (5)*
C(1)	1618 (7)	6127 (12)	6706 (7)	18 (5)*
C(2)	1090 (10)	4990 (17)	5802 (8)	48 (8)*
C(3)	2082 (8)	8142 (13)	8016 (7)	24 (6)*
C(4)	2289 (11)	9722 (15)	8790 (9)	49 (8)*
C(17)	2963 (7)	7477 (12)	6344 (6)	15 (4)
C(42)	2105 (7)	5053 (11)	8478 (6)	9 (3)

[a] Parameters for phenyl groups, hexafluorophosphates, and dichloromethane are omitted (see supplementary material). [b] For values marked with an asterisk, equivalent isotropic *U* is defined as one-third of the trace of the orthogonalized U_{ij} tensor.

Table III. Atomic Coordinates (×10⁴) and Isotropic Thermal Parameters (Å² × 10³) for $[Ir(CNCH_3)_3Au(\mu\text{-dpm})_2](PF_6)_2$[a] (**3**)

	x	*y*	*z*	*U*[b]
Ir(1)	1351 (1)	932 (1)	1244 (1)	15 (1)*
Au(1)	1282 (1)	3029 (1)	1255 (1)	17 (1)*
P(1)	1992 (2)	1392 (4)	943 (2)	19 (2)*
P(2)	2019 (2)	3441 (4)	1428 (2)	22 (2)*
P(3)	533 (2)	3233 (4)	1074 (2)	14 (2)*
P(4)	678 (2)	1129 (4)	1529 (2)	20 (2)*
N(1)	719 (5)	1022 (12)	280 (5)	18 (6)*
N(2)	1932 (5)	1171 (13)	2233 (5)	28 (6)*
N(3)	1435 (6)	−1420 (14)	1244 (7)	41 (8)*
C(1)	968 (6)	1032 (17)	620 (7)	28 (8)*
C(2)	441 (6)	1037 (18)	−156 (6)	31 (9)*
C(3)	1700 (6)	1099 (15)	1885 (7)	28 (8)*
C(4)	2198 (9)	1221 (18)	2690 (7)	59 (11)*
C(5)	1416 (7)	−624 (15)	1265 (8)	32 (8)*
C(6)	1406 (17)	−2496 (17)	1275 (14)	181 (25)*
C(19)	2338 (5)	2354 (12)	1282 (6)	13 (5)
C(44)	279 (5)	2007 (16)	1201 (5)	14 (4)

[a] Parameters for phenyl groups and hexafluorophosphates are omitted (see supplementary material). [b] For values marked with an asterisk, equivalent isotropic *U* is defined as one-third of the trace of the orthogonalized U_{ij} tensor.

(14) Casalnuovo, A. L.; Pignolet, L. H.; van der Velden, J. W. A.; Bour, J. J.; Steggerda, J. J. *J. Am. Chem. Soc.* **1983**, *105*, 5957.
(15) Casalnuovo, A. L.; Laska, T.; Nilsson, P. D.; Olofson, J.; Pignolet, L. H. *Inorg. Chem.* **1985**, *24*, 233.
(16) Casalnuovo, A. L.; Casalnuovo, J. A.; Nilsson, P. V.; Pignolet, L. H. *Inorg. Chem.* **1985**, *24*, 2554.
(17) Casalnuovo, A. L.; Laska, T.; Nilsson, P. V.; Olofson, J.; Pignolet, L. H.; Bos, W.; Bour, J. J.; Steggerda, J. J. *Inorg. Chem.* **1985**, *24*, 182.
(18) Luke, M. A.; Mingos, M. P.; Sherman, D. J.; Wardle, R. W. M. *Transition Met. Chem.* **1987**, *12*, 37.
(19) Balch, A. L.; Nagle, J. K.; Oram, D. E.; Reedy, P. E., Jr. *J. Am. Chem. Soc.* **1988**, *110*, 454.
(20) Balch, A. L.; Catalano, V. J.; Olmstead, M. M. *J. Am. Chem. Soc.* **1990**, *112*, 2010.

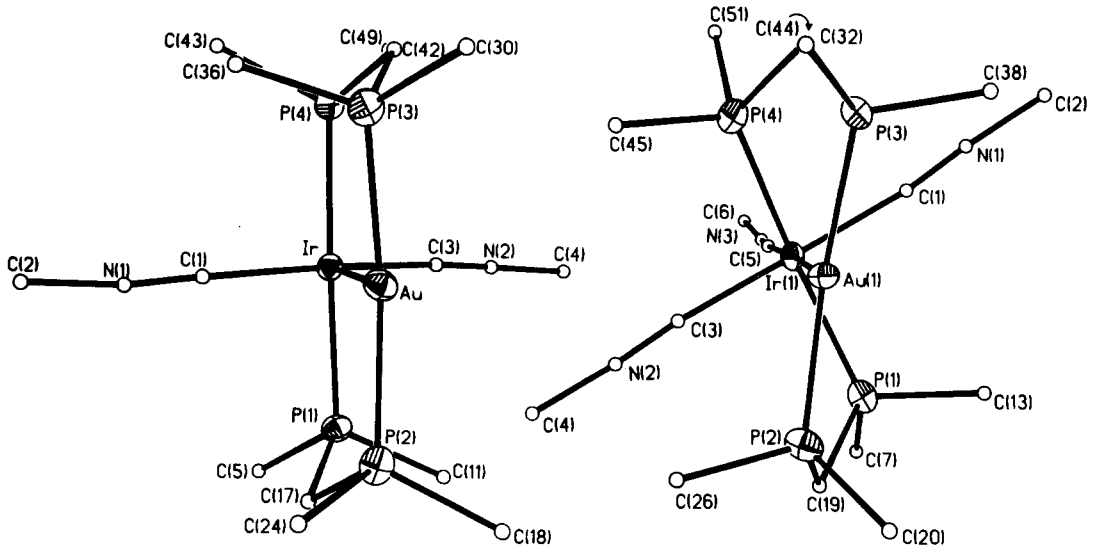

Figure 2. Comparison of the inner cores of $[Ir(CNMe)_2Au(\mu\text{-dpm})_2](PF_6)_2$ (**2**) (left) and $[Ir(CNMe)_3Au(\mu\text{-dpm})_2](PF_6)_2$ (**3**) (right).

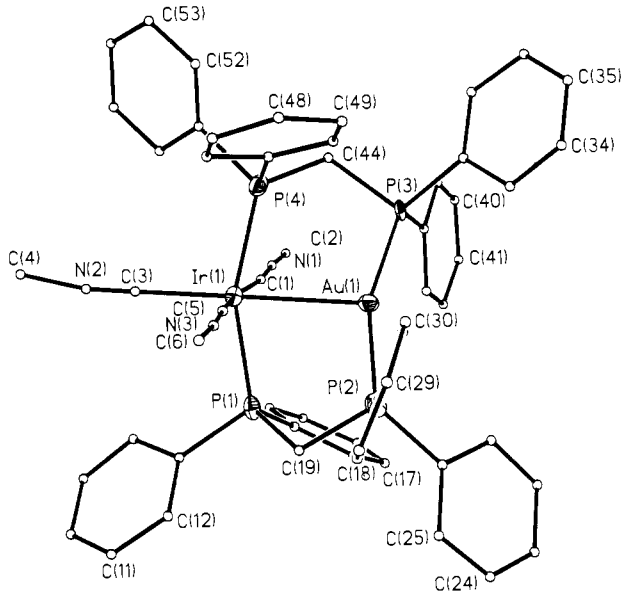

Figure 3. Structure of the cation in $[Ir(CNMe)_3Au(\mu\text{-dpm})_2](PF_6)_2$ (**3**).

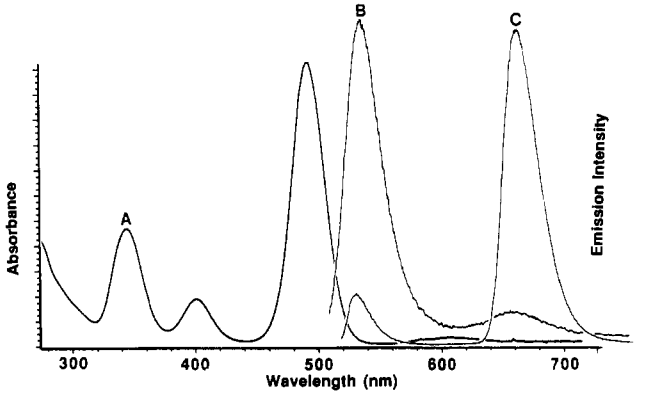

Figure 4. Electronic absorption (A) and uncorrected emission (B) spectra of $[Ir(CNMe)_2Au(\mu\text{-dpm})_2](PF_6)_2$ (**2**) in dichloromethane at 25 °C. Trace C shows the emission spectrum obtained from a frozen solution at −196 °C.

toward the side of the chloride ligand. Despite these displacements, they do not appear large enough to involve an additional bridging interaction with either the isocyanide or chloride ligands that are adjacent to the displacement.

Structure of $[Ir(CNCH_3)_3Au(\mu\text{-dpm})_2](PF_6)_2$ (3). The asymmetric unit consists of the cation and two normal hexafluorophosphate anions. The complex has no crystallographically imposed symmetry. A drawing of the cation is shown in Figure 3. Selected bond angles and distances are shown in Table I, where they may be compared to those of **2**. Atomic coordinates are given in Table III.

The cation is **3** is clearly related to that in **2** by the addition of one isocyanide ligand to the vacant axial coordination site on iridium. That addition has produced a number of profound structural changes. Most significantly, the Ir–Au distance has decreased by 0.127 Å to 2.817 (1) Å, so that it is just at the long end of the range seen for Ir–Au single bonds.[14-20]

The $IrAu(\mu\text{-dpm})_2$ core has become twisted, and the ring within this unit exists as a twisted chair form. Figure 2 shows corresponding views of the inner cores of **2** and **3** that emphasize the twisting in **3**. The dihedral angle between the P(3)AuIr and P(4)IrAu planes is 34.0°, and the dihedral angle described by the planes P(1)AuIr and P(2)AuIr is 34.5°. The trans P–Ir–P and P–Au–P units are no longer linear but bend inward toward each other. The P(1)–Ir–P(4) angles is 152.2 (2)°, and the P(2)–Au–P(3) angle is 159.2 (2)°. The P(1)–Ir–Au and P(4)–Ir–Au angles (79.1 (1) and 79.2 (1)°, respectively) are significantly less than 90°. Conversely, the P(2)–Au–Ir and P(3)–Au–Ir angles (99.8 (2) and 101.0 (1)°, respectively) are greater than 90°. This twisting allows the iridium and gold ions to approach each other without much bending of the P–C–P angles within the dpm bridges. Thus, the P–C–P angles in **2** are 115.0 (2) and 115.2 (7) while they are 113.4 (9) and 113.6 (8)° in **3**. Consequently, the nonbonded P···P separations are similar in both **2** and **3**.

The metal–ligand and intraligand bond distances in **3** all fall within normal limits. It is significant, however, that the axial Ir–C(5) distance in **3** is somewhat longer than the other Ir–C distances. This elongation results from the high structural trans effect of the Au–Ir bond.

Electronic Absorption and Emission Spectra. Relevant spectra for **2** are shown in Figure 4. The absorption spectrum (trace A) is dominated by a strong band at 492 nm (ϵ = 5100 M^{-1} cm^{-1}), which is assigned to the allowed $\sigma^*(d_{z^2}d_{z^2}) \rightarrow \sigma(p_zp_z)$ transition (vide infra). The weak band at 608 nm (ϵ = 90 M^{-1} cm^{-1}) is believed to be the spin-forbidden counterpart of the 492-nm transition. Two other bands at 400 nm (ϵ = 920 M^{-1} cm^{-1}) and 344 nm (ϵ = 2300 M^{-1} cm^{-1}) are also observed. Trace B represents the emission data gathered from a dichloromethane solution of the complex at 298 K with excitation at 492 nm. There is a strong emission at 540 nm along with a weaker emission at 668 nm. The lifetime of the emissions at 668 and 540 in dichloromethane at 298 K are less than 15 ns. When the sample is cooled to 77 K (trace C), the 540-nm band shifts to slightly higher energy (535 nm) and the low-energy feature at 668 nm grows in intensity relative to the 535-nm band. Examination of the excitation profile

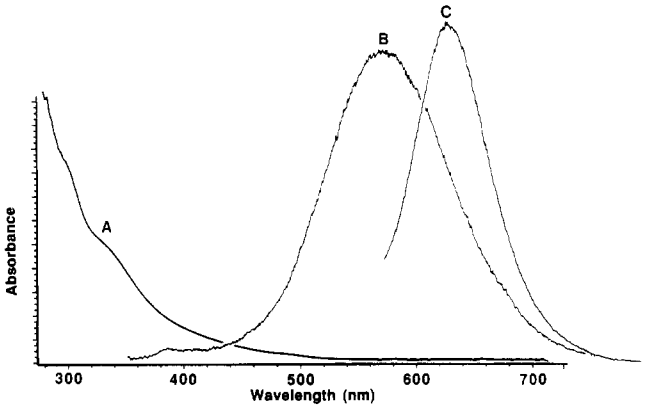

Figure 5. Electronic absorption (A) and uncorrected emission (B) spectra of a dichloromethane solution of $[Ir(CNMe)_3Au(\mu\text{-dpm})_2](PF_6)_2$ (**3**). Trace C shows the emission spectrum obtained from a frozen solution at −196 °C.

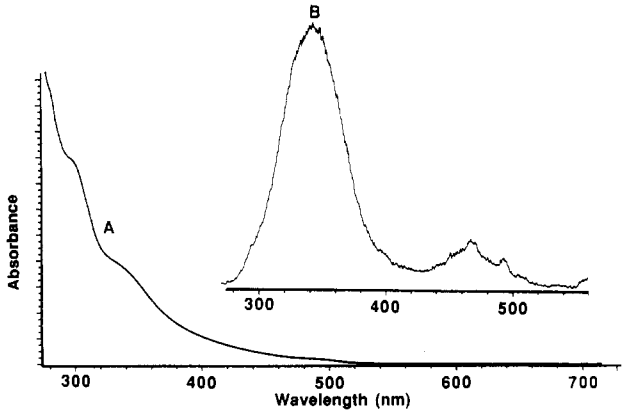

Figure 6. Electronic absorption spectrum of $[Ir(CNMe)_3Au(\mu\text{-dpm})_2](PF_6)_2$ in dichloromethane along with the excitation profile (B) obtained for the emission at 580 nm.

at 77 K reveals that the emission at 670 nm is excited by absorption at either 608 or 492 nm. At 77 K the lifetime of the 668-nm emission is 4.4 μs while that of the 540-nm emission is still less than 15 ns. These spectral features are very similar to those of $[Ir(CO)ClAu(\mu\text{-dpm})_2]^+$. On the basis of its lifetime and mirror image relationship to the absorption, the emission band at 540 nm is assigned to a fluorescent process while the lower energy emission with the larger Stokes' shift and longer lifetime (at 77 K) is assigned as phosphorescence. The decrease in relative intensity and lifetime of the 688-nm emission on warming the sample is taken as temperature-dependent quenching of the phosphorescence.

The absorption and emission spectra for **3** are compared in Figure 5. The absorption spectrum in dichloromethane shows that the prominent feature of **2**, the 492-nm absorption, is lost and a much less well-defined spectrum results with two shoulders at 332 nm (ϵ = 6700 M^{-1} cm^{-1}) and 298 (ϵ = 11000 M^{-1} cm^{-1}) as the only discernable features. The emission spectrum obtained from dichloromethane solution at 25 °C is shown in trace B. It consists of a broad feature with λ_{max} at 580 nm and a less prominent feature at 386 nm. The lifetime at 25 °C is 1.2 μs for the 580-nm emission and less than 15 ns for the 386-nm emission. An excitation profile of the 580-nm emission is shown in trace B of Figure 6, where it is compared with the absorption spectrum (trace A). This shows that the emission is pumped by two bands, one at 460 nm and the other at 345 nm. When the solution is cooled to −196 °C, the 386-nm feature can no longer be detected, while the low-energy feature sharpens and shifts to 628 nm. Its lifetime is 4.8 μs. On the basis of the lifetime and large Stokes', shift this feature is attributed to phosphorescence.

Discussion

The shortening of the Ir–Au distance observed when methyl isocyanide is added to **2** to form **3** and the pronounced spectral changes that accompany this shortening are indicative of a major change in the Ir–Au bonding within the binuclear complexes. The Ir–Au bonding in **2** can be readily viewed in the context of bonding schemes developed for d^8d^8 dimers[1-4] with the realization that one d^{10} center substitutes for one of the d^8 metal ions. A qualitative molecular orbital diagram for **2** is shown on the right side of Figure 7. This diagram focuses on the gold- and iridium-filled d_{z^2} and empty p_z orbitals, which are directed nearly along the Au–Ir axis. This interaction leads to filled $\sigma(d_{z^2})$ and $\sigma^*(d_{z^2})$ orbitals. Mixing these with the empty $\sigma(p_z)$ and $\sigma^*(p_z)$ orbitals results in stabilization of both the $\sigma(d_{z^2})$ and $\sigma^*(d_{z^2})$ levels, so that the net interaction is attractive between gold and iridium, despite the fact that both the bonding and antibonding orbitals are filled.[1,3,4] The intense absorption feature at 492 nm is due to an electronic transition from the $\sigma^*(d_{z^2})$ to the $\sigma(p_z)$ level. This band has characteristic counterparts in the spectra of most d^8d^8 complexes (the proximity-shifted band).[4] This picture has, by focusing on the metal orbitals, omitted reference to the strong π-back-bonding capabilities of the isocyanide ligands. We believe that they are involved as substantial π-acceptors but that their effect is secondary to the metal–metal interactions. In this context, note the similarities in the pattern of the electronic absorption and emission spectra of **1**[11] with one π-acceptor (carbon monoxide) and one π-donor (chloride) ligand on iridium with **2** with two π-acceptor (isocyanide) ligands in their place.

Addition of a ligand (the axial methyl isocyanide) to the axial coordination site of the iridium ion in these binuclear complexes has two effects on the σ-bonding. It removes the empty p_z orbital from the picture shown on the right side of Figure 7. That orbital is now involved in forming the new Ir–C σ-bond. It also raises the energy of the filled d_{z^2} orbital. In turn these changes result in alteration of the Ir–Au bonding. As shown on the left side of Figure 7, the major bonding in **3** involves donation of a pair of electrons from the filled d_{z^2} orbital on iridium into an empty p_z

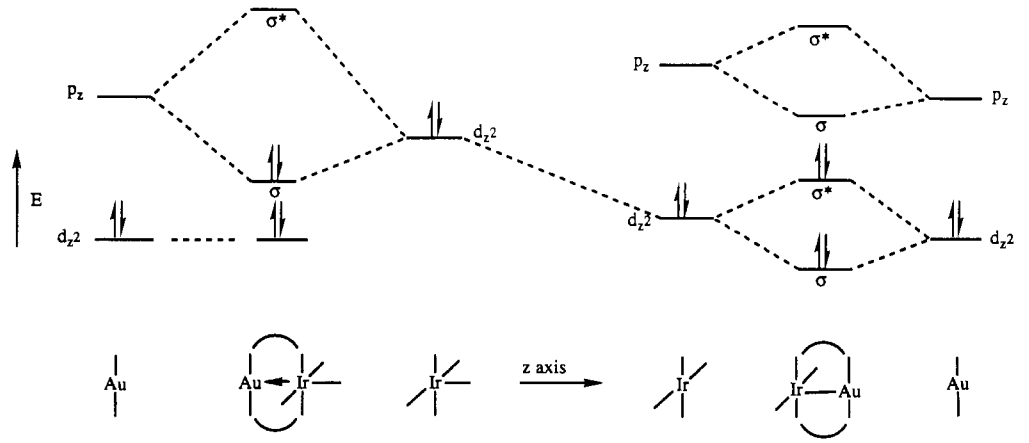

Figure 7. Qualitative molecular orbital diagrams for **2** and **3**.

Table IV. Crystal Data and Data Collection Parameters for **2** and **3**

	2	**3**
	$[Ir(CNCH_3)_2Au(\mu\text{-dpm})_2](PF_6)_2\cdot CH_2Cl_2$	$[Ir(CNCH_3)_3Au(\mu\text{-dpm})_2](PF_6)_2$
formula	$C_{55}H_{50}N_2AuIrF_{12}P_6Cl_2$	$C_{56}H_{53}N_3AuIrF_{12}P_6$
fw	1612.9	1570.6
color and habit	red blocks	yellow blocks
crystal system	monoclinic *p*	monoclinic *c*
space group	$P2_1/c$ (No. 14)	$C2/c$
a, Å	20.337 (4)	30.511 (8)
b, Å	12.633 (2)	13.393 (4)
c, Å	22.523 (5)	28.859 (8)
β, deg	100.29 (1)	99.10 (2)
V, Å^3	5693 (2)	11764 (8)
T, K	130	130
Z	4	8
cryst dimens, mm	0.38 × 0.12 × 0.22	0.75 × 0.30 × 0.25
d_{calcd}, g cm^{-3}	1.88	1.77
radiation, Å	Mo Kα (λ = 0.71069)	Mo Kα (λ = 0.71069)
μ(Mo Kα), cm^{-1}	53.82	51.69
range of transm factors	0.15–0.58	0.040–0.20
no. of data collected	8230	8251
no. of unique data	4998	7605
	R(merge) = 0.007	R(merge) = 0.009
no. of data refined	4981 [$I > 4\sigma(I)$]	4730 [$I > 4\sigma(I)$]
no. of params refined	450	462
R^a	0.0572	0.0698
$R_w{}^a$	0.055 [$w = 1/(\sigma^2F_o)$]	0.0534 [$w = 1/(\sigma^2F_o)$]

$^a R = \sum||F_o| - |F_c||/|F_o|$ and $R_w = \sum||F_o| - |F_c||w^{1/2}/\sum|F_o w^{1/2}|$.

orbital on gold. Thus, the metal–metal bonding is converted into one of a dative, donor–acceptor type. Since only the Ir–Au σ-bonding orbital is filled, and its antibonding counterpart is empty, the Ir–Au bond is strengthened and shortened. The prominent $\sigma^*(d_{z^2}) \rightarrow \sigma(p_z)$ transition in **2** is lost, but a new band tentatively assigned to the $\sigma \rightarrow \sigma^*$ transition now occurs at significantly higher energy in **3**. Although this transition appears as only a shoulder in the absorption spectrum, it is much more readily distinguished in the excitation spectrum shown in Figure 6.

The emission seen in Figure 5 for **3** is characterized as arising from a triplet state. This is supported by the lifetime of this state, its large Stokes' shift, and its temperature dependence. As seen in Figure 5, the emission dramatically sharpens and λ_{max} moves to lower energy on cooling. Striking narrowing of emissive bands have previously been reported for other binuclear complexes with one electron in a σ^* orbital of a metal–metal-bonded species.[21] Thus it is likely that the excited state involved in this has the $\sigma^1\sigma^{*1}$ configuration. However, it is also well recognized that many mononuclear gold(I) complexes luminesce,[8] and there is, with the available data, no assurance that the observed emission arises from states affecting the metal–metal bonding within **3**.

There are significant precedents for the formation of donor–acceptor metal–metal bonds of the type proposed for **3**. $Os(CO)_4(PR_3)$, which is isoelectronic with a $Ir(CNMe)_3P_2^+$ fragment, is capable of forming unsupported dative bonds to chromium, tungsten, and osmium.[22] Because of its charge and the higher metal oxidation state, the $Ir(CNMe)_3P_2^+$ unit would be expected to be a poorer donor than the osmium complex, but the presence of the two dpm bridges serves to facilitate bonding to the adjacent gold(I). There are also several other cases of dpm-bridged binuclear complexes in which the metal–metal bonding has been described in terms of a donor–acceptor bond.[23]

The asymmetry in these gold/iridium complexes plays a major role in controlling the ligand addition and metal–metal bond changes. In **2** the iridium atom retains the affinity for an added ligand in much the same way as in a simple mononuclear, planar iridium(I) complex. However, the effect of addition of a ligand is transmitted through the iridium so that the iridium–gold bonding is altered.

Experimental Section

Preparation of Compounds. $[Ir(CO)ClAu(\mu\text{-dpm})_2](PF_6)$,[13] $[Ir(COD)Cl]_2$,[24] and methyl isocyanide[25] were prepared by published methods.

$[Ir(CNMe)_2Au(\mu\text{-dpm})_2](PF_6)_2$ (2). Methyl isocyanide (2.4 mg, 0.082 mmol) was added to a solution of 57 mg (0.041 mmol) of $[Ir(CO)ClAu(\mu\text{-dpm})_2](PF_6)$ in 10 mL of acetone. The color of the solution changed from bright orange to pale yellow. Addition of a solution of 20 mg (0.123 mmol) of ammonium hexafluorophosphate in 25 mL of methanol caused the solution to turn green. After the solution was stirred for 20 min, the volume of the solution was reduced to yield green crystals. The product was collected by filtration and recrystallized from dichloromethane/2-propanol (yield: 76%).

$[Ir(CNCH_3)_3Au(\mu\text{-dpm})_2](PF_6)_2$. A three-neck round-bottom flask equipped with an addition funnel and a condensor was charged with 100 mg (0.149 mmol) of $[Ir(COD)Cl]_2$ and 229 mg (0.596 mmol) of dpm. A 50-mL aliquot of degassed dichloromethane was added via cannula to form a bright yellow solution. Methyl isocyanide (36.6 mg, 0.900 mmol) was added, and the solution was stirred for 10 min. A solution of 147 mg (0.298 mmol) of Ph_3PAuCl dissolved in CH_2Cl_2 was added dropwise to the stirred yellow solution. After the addition, the slightly orange solution was heated under reflux for 1 h. After this was cooled to room temperature, 100 mg (0.613 mmol) of ammonium hexafluorophosphate dissolved in 30 mL of methanol was added. The volume was reduced to yield the yellow crystalline salt, which was collected by filtration, washed with methanol, and vacuum dried.

Physical Measurements. The $^{31}P\{^1H\}$ NMR spectra were recorded on a General Electric QE-300 NMR spectrometer that operates at 121.7 MHz with an external 85% phosphoric acid standard and the high field positive convention for reporting chemical shifts. Infrared spectra were recorded on an IBM IR32 spectrometer. Electronic spectra were recorded with a Hewlett-Packard 8450A spectrometer. Uncorrected emission spectra were obtained through the use of a Perkin-Elmer MPF-44B fluorescence spectrometer.

Standard laser-induced fluorescence (LIF) techniques were employed to measure excited-state lifetimes with 355- and 503-nm (Raman-shifted 355-nm) excitation from a Nd:YAG laser, operating as described previously.[26] In each case, the solvent was CH_2Cl_2 freshly distilled from

(21) Stiegman, A. E.; Miskowski, V. M. *J. Am. Chem. Soc.* **1988**, *110*, 4053.
(22) Einstein, F. W. B.; Jones, T.; Pomeroy, R. K.; Rushman, P. *J. Am. Chem. Soc.* **1984**, *106*, 2707. Davis, H. B.; Einstein, F. W. B.; Glavina, P. G.; Jones, T.; Pomeroy, R. K.; Rushman, P. *Organometallics* **1989**, *8*, 1030. Batchelor, R. J.; Davis, H. B.; Einstein, F. W. B.; Pomeroy, R. K. *J. Am. Chem. Soc.* **1990**, *112*, 2036.
(23) Brown, M. P.; Cooper, S. J.; Frew, A. A.; Manojlović-Muir, L.; Muir, K. W.; Puddephatt, R. J.; Seddon, K. R.; Thomson, M. A. *Inorg. Chem.* **1981**, *20*, 1500. Ladd, J. A.; Olmstead, M. M.; Balch, A. L. *Inorg. Chem.* **1984**, *23*, 2318.
(24) Crabtree, R. H.; Qwirk, J. M.; Felkin, H.; Fillebeen-Khan, T. *Synth. React. Inorg. Met. Org. Chem.* **1982**, *12*, 407.
(25) Schuster, R. E.; Scott, J. E.; Casanova, J., Jr. *Org. Synth.* **1966**, *46*, 75.

CaH_2. Sample concentrations were on the order of 10^{-4} M. Solvent was degassed by using four freeze-pump-thaw cycles.

X-ray Data Collection for $[Ir(CNCH_3)_2Au(\mu\text{-dpm})_2](PF_6)_2\cdot CH_2Cl_2$. The blocklike crystals were formed by slow diffusion of 2-propanol into a methylene chloride solution of $[Ir(CNCH_3)_2Au(\mu\text{-dpm})_2](PF_6)_2$. To prevent cracking, the crystal was coated with light hydrocarbon oil. The crystal was mounted on a glass fiber with silicon grease and placed into the 130 K nitrogen stream of a Syntex $P2_1$ diffractometer with a modified LT-1 low-temperature apparatus. Unit cell parameters were determined by least-squares refinement of 10 reflections with $10.8 < 2\theta < 16.8°$. The parameters were verified by examination of axial photos. This refinement yielded the monoclinic crystal system. The unique space group $P2_1/c$ (No. 14) was determined by the following conditions: $h00$, $h = 2n$; $0k0$, $k = 2n$; $00l$, $l = 2n$. The two check reflections remained stable throughout the data collection. The data were corrected for Lorentz and polarization effects. Crystal data are given in Table IV. Scattering factors and corrections for anomalous dispersion were taken from a standard source.[27]

Solution and Structure Refinement for $[Ir(CNCH_3)_2Au(\mu\text{-dpm})_2](PF_6)_2\cdot CH_2Cl_2$. Calculations were performed on a Data General MW/10000 computer. The structure was solved in the centrosymmetric space group $P2_1/c$ (No. 14), and heavy atom positions for Ir and Au were assigned via the Patterson function. All non-carbon atoms and the isocyanide carbons, C(1) to C(4), were refined with anisotropic thermal parameters, while all others were left isotropic. Hydrogens were fixed to all carbons where chemically justified, except the solvent carbon, C(55). The hydrogen atom positions were calculated by using a riding model with C-H vector fixed at 0.96 Å and a thermal parameter 1.2 times the host carbon. The largest unassigned peak in the final difference map had density equal to 1.65 e/Å^3. This peak is 1.38 Å from C(12). Absorption corrections were applied,[28] and the structure was refined to convergence. The goodness of fit was calculated at 1.076 with a mean (shift/esd) of 0.010 for the overall scale.

X-ray Data Collection for $[Ir(CNCH_3)_3Au(\mu\text{-dpm})_2](PF_6)_2$. The blocklike crystals were formed by slow diffusion of diethyl ether into a methylene chloride solution of $[Ir(CNCH_3)_3Au(\mu\text{-dpm})_2](PF_6)_2$. To prevent cracking, the crystal was coated with light hydrocarbon oil. The crystal was handled as described above. Unit cell parameters were determined by least-squares refinement of 12 reflections with $27.2 < 2\theta < 31.2°$. The parameters were verified by examination of axial photos. This refinement yielded the monoclinic crystal system. The unique space group $C2/c$ (No. 15) was determined by the conditions hkl, $h + k = 2n$ and $l = 2n$. The two check reflections remained stable throughout the data collection. The data were corrected for Lorentz and polarization effects. Crystal data are given in Table IV.

Solution and Structure Refinement for $[Ir(CNCH_3)_3Au(\mu\text{-dpm})_2](PF_6)_2$. Calculations were performed on a Data General MV/10000 computer. The structure was solved in the centrosymmetric space group $C2/c$, and heavy atom positions (Ir and Au) were assigned via the Patterson function. All non-carbon atoms and the methyl isocyanide carbon atoms were refined with anisotropic thermal parameters, while all others were left isotropic. Hydrogens were treated as described above. Large thermal motion is seen in the terminal carbon (C(6)) of the methyl isocyanide trans to Au(1). To verify assignment as a single methyl group and not a disordered unit, the address was removed, and the structure was refined. Subsequent inspection of a Fourier difference map produced only one peak in the same location, thus verifying the assignment. The largest unassigned peak in the final difference map had density equal to 2.91 e/Å^3. This peak is 1.26 Å from Au(1). Absorption corrections were applied, and the structure was refined to convergence. The goodness of fit was calculated at 1.697 with a mean (shift/esd) of 0.010 for the overall scale.

Acknowledgment. We thank the National Science Foundation (Grant CHE-8941209) for support, Johnson-Matthey, Inc., for a loan of iridium salts, Professor P. B. Kelly for assistance in measuring the emission lifetimes, and Dr. Marilyn Olmstead, B. Noll, and E. Fung for crystallographic assistance.

Supplementary Material Available: Tables of atomic positional parameters, bond distances, bond angles, anisotropic thermal parameters, and hydrogen atom positions for **2** and **3** (10 pages); listings of structure factors for **2** and **3** (53 pages). Ordering information is given on any current masthead page.

(26) Balch, A. L.; Catalano, V. J.; Olmstead, M. M. *J. Am. Chem. Soc.* **1990**, *112*, 7558.
(27) *International Tables for X-ray Crystallography*; Kynoch: Birmingham, England, 1974; Vol. 4.
(28) The method obtains an empirical tensor from an expression relating F_o and F_c: Moezzi, B. Ph.D. Thesis, University of California, Davis, 1987.

Contribution from the Departments of Chemistry, Princeton University, Princeton, New Jersey 08544, and Colorado State University, Fort Collins, Colorado 80523

Analysis of a Siroheme Model Compound: Core-Size Dependence of Resonance Raman Bands and the Siroheme Spin State in Sulfite Reductase

Dan Melamed,[†] Eric P. Sullivan, Jr.,[‡] Kristine Prendergast,[†] Steven H. Strauss,[‡] and Thomas G. Spiro*,[†]

Received July 27, 1990

Resonance Raman (RR) and infrared spectra are reported for nickel(II) octaethylisobacteriochlorin (OEiBC) and its $^{15}N_4$ and *meso*-d_3 isotopomers. The bands are assigned to porphyrin-like modes with the aid of a normal-coordinate analysis by using a force field developed for nickel octaethylporphyrin (OEP) and by scaling the force constants to bond lengths expected on the basis of the crystal structure of nickel *meso*-tetramethylisobacteriochlorin. The eigenvectors show a relationship between OEP and OEiBC modes, despite some localization to one or the other half of the OEiBC ring caused by the unequal lengths of the methine bridge bonds adjacent to the pyrrole and pyrroline rings. Excitation at wavelengths near the B and Q absorption bands show Q-resonant RR spectra to be dominated by a single Franck-Condon active mode, ν_{29}, for NiOEiBC, in contrast to the vibronic scattering from many modes seen in porphyrins. On the other hand, B-resonant spectra that are dominated by Franck-Condon active modes for porphyrins show equally strong enhancement of vibronic modes in NiOEiBC. These differences are attributed to the energy separation of the a_{1u} and a_{2u} HOMO's, brought about by pyrrole ring reduction, and the resultant diminution of effects which are associated with configuration interaction. When the vibrational assignments are used to track the RR bands of a series of iron-OEiBC complexes, a distinctive dependence of the high-frequency bands on the ring core size of the porphyrin analogues is observed, although the slopes of the correlations differ from those reported previously for porphyrin or chlorin. Direct comparison of the iron-OEiBC high-frequency bands with those of the *Escherichia coli* sulfite reductase hemoprotein confirms the previous inference that the iron(II) siroheme is intermediate spin in the semireduced protein but high spin in the fully reduced protein.

Introduction

Resonance Raman (RR) spectroscopy, a well-established technique for studying structure and dynamics in metalloporphyrins and heme proteins,[1] is increasingly being extended to reduced porphyrins,[2-6] especially in connection with the structural analysis of chlorophyll and chlorin-containing proteins. Although

* Author to whom correspondence should be addressed.
[†] Princeton University.
[‡] Colorado State University.

(1) Spiro, T. G.; Li, X. Y. In *Biological Applications of Raman Spectroscopy*; John Wiley: New York, 1988; Vol. II.
(2) Schick, G. A.; Bocian, D. F. *Biochim. Biophys. Acta* **1987**, *895*, 127.
(3) Andersson, L. A.; Loehr, T. M.; Stershic, M. T.; Stolzenberg, A. M. *Inorg. Chem.* **1990**, *29*, 2278.
(4) Kitagawa, T.; Ozaki, Y. *Struct. Bonding (Berlin)* **1987**, *64*, 1.

0020-1669/91/1330-1308$02.50/0